Journal of Power Sources 244 (2013) 109–114

Contents lists available at SciVerse ScienceDirect

Journal of Power Sources

journal homepage: www.elsevier.com/locate/jpowsour

A simple electrochemical cell for *in-situ* fundamental structural analysis using synchrotron X-ray powder diffraction

William R. Brant [a], Siegbert Schmid [a,*], Guodong Du [b], Qinfen Gu [c], Neeraj Sharma [d,e]

[a] School of Chemistry, The University of Sydney, Sydney, NSW 2006, Australia
[b] Institute for Superconducting & Electronic Materials, University of Wollongong, Innovation Campus, Squires Way, Fairy Meadow, NSW 2519, Australia
[c] Australian Synchrotron, 800 Blackburn Rd, Clayton, VIC 3168, Australia
[d] Australian Nuclear Science and Technology Organisation, Locked Bag 2001, Kirrawee DC, NSW 2232, Australia
[e] School of Chemistry, The University of New South Wales, Sydney, NSW 2052, Australia

HIGHLIGHTS

- Developed *in-situ* cell for fundamental structural analysis using synchrotron X-ray powder diffraction.
- Cell constructed in-house using readily available materials.
- Cell tested at the Australian Synchrotron's powder diffraction beamline.
- Continuous collection of diffraction data during cycling enabled kinetic analysis.
- Three distinct discharge regions identified for $Li_{0.18}Sr_{0.66}Ti_{0.5}Nb_{0.5}O_3$.

ARTICLE INFO

Article history:
Received 30 October 2012
Received in revised form
8 March 2013
Accepted 11 March 2013
Available online 25 March 2013

Keywords:
In-situ X-ray diffraction
In-situ electrochemical cell
Defect perovskite
Lithium insertion
Kinetic analysis

ABSTRACT

A simple *in-situ* cell design is formulated based on the various *in-situ* electrochemical cells developed over the last three decades. The cell is targeted at those researchers who are not necessarily in the field of lithium ion battery research but are interested in synthesising and performing fundamental structural analyses of compounds that cannot be made via any other route. Therefore, this design uses only components that are routinely available and can be machined in-house. The effectiveness of the initial cell design is demonstrated through kinetic analysis of the lithium insertion reaction for the $Li_{0.18}Sr_{0.66}Ti_{0.5}Nb_{0.5}O_3$ defect perovskite using data obtained from hundreds of diffraction patterns. Within the first discharge it has been possible to identify three regions with different rates of crystal lattice expansion. These regions extend from 1.01 to 1.47 V, 1.47–1.58 V and 1.58–2.07 V with rates of crystal lattice expansion determined to be $1.765(6) \times 10^{-5}$ Å min^{-1}, $1.44(5) \times 10^{-5}$ Å min^{-1} and $2.47(1) \times 10^{-5}$ Å min^{-1}, respectively. These three regions correlate with three distinct regions in the electrochemical profile, between 1.00 and 1.36 V, 1.36–1.55 V and 1.55–1.80 V.

1. Introduction

As the importance of lithium ion battery technology continues to grow dramatically, careful screening and investigations of battery materials are essential for continued development. A vital part of this is an understanding of how the crystal structures of electrode materials affect the resulting properties of a battery. Given this necessity and also the complex nature of lithium insertion reactions, *in-situ* studies were undertaken relatively early on in the investigation of lithium ion battery technology. In particular, as it became clear that structural changes in both the anode and cathode played an important role in overall battery performance, *in-situ* X-ray diffraction became an essential tool in understanding the processes which occur during the operation of a rechargeable lithium ion battery. *In-situ* X-ray diffraction during the electrochemical insertion/extraction of lithium, or any other small cations, does not necessarily need to be applied to battery materials alone. For example, tailored electrochemical syntheses and the formation characteristics of new metastable phases, which cannot be synthesised via conventional means, can be probed, (*e.g.*, CoO_2 [1] and λ-MnO_2 [2]). Therefore, *in-situ* investigations using an electrochemical cell can provide a unique means of following the formation of new materials as well as detailing the relationship between

* Corresponding author. Tel.: +61 2 93514196; fax: +61 2 93513329.
E-mail address: siegbert.schmid@sydney.edu.au (S. Schmid).

0378-7753/$ – see front matter
http://dx.doi.org/10.1016/j.jpowsour.2013.03.086

electrode structure and properties. In order to create a cell specially designed for *in-situ* investigations, the advantages and disadvantages of existing cells must be considered. Thus, this contribution discusses various *in-situ* X-ray cell types which have been designed and, by considering the merits of each, proceeds to describe and evaluate our *in-situ* X-ray diffraction cell design. The design is specifically targeted at those researchers who are primarily interested in materials produced via electrochemical synthesis.

1.1. Overview of previous in-situ cell designs

One of the most important factors to consider when designing an *in-situ* cell is what diffraction instruments are available. Broadly, there are two different types of X-ray diffraction geometries available for *in-situ* work, reflection and transmission. In reflection mode, X-rays are targeted at an angle θ to a flat sample and reflected to a detector at a fixed distance from the point of diffraction. As most conventional X-ray diffractometers incorporate reflection geometry, early *in-situ* experiments were typically carried out in reflection mode.

The first *in-situ* study was performed by Chianelli et al. investigating structural changes induced by lithium insertion into the Li–TiS_2 system [3]. In order to allow for the passage of X-rays into their cell they used either a beryllium or polyethylene window. A similar design was then utilised by Dahn et al. who used an electrochemical cell comprised of two stainless steel plates with a recess for a beryllium window on one side. The positive electrode was painted directly onto the beryllium window, and the cell also contained a lithium metal anode, an electrolyte soaked separator and a polypropylene gasket to prevent contact between the electrodes and ensure a hermetic seal [4]. The benefit of using a beryllium window, besides being relatively transparent to X-rays, is that it provides a hard surface which can be used to ensure good contact of the cell components whilst keeping the entire electrode flat. This is especially important in reflection geometry where, in order to obtain a high quality diffraction pattern, the sample needs to be flat and in a fixed position relative to the detector. Thus, the rigid beryllium window ensures a well-defined, flat reference plane. Most *in-situ* cells used in reflection geometry, often with conventional X-ray diffractometers, have made use of beryllium windows for this reason [5]. The main disadvantage of using a beryllium window is that it cannot be used in contact with electrode materials above 4.2 V *vs.* Li metal due to beryllium oxidising and becoming porous. This limits the range of cathode materials that can be investigated using beryllium windows. In order to overcome this disadvantage several design changes were made. The major design change, which remains most common, is the use of a spacer ring to introduce an air gap between the beryllium window and the electrochemically active part of the cell [1]. Although this introduces some additional complexity to the construction of the cell it can still be used in most *in-situ* cell designs, *e.g.*, those based on coin cells [6] or Swagelok™ type cells [5]. The second geometry used for *in-situ* diffraction experiments, transmission mode, places the sample normal to the direction of the beam such that the beam passes through the cell and a diffraction pattern is collected on the other side. Thus, for transmission geometry it is more challenging to design *in-situ* cells as the X-ray beam must be able to pass through every component of the cell and still produce a diffraction pattern with sufficient intensity for analysis. However, this feature also means that the entire thickness of the cell is probed during the experiment, not just the surface layers of the material as is the case in reflection mode. As a result, there will be contributions to the pattern from other cell components. This is not a major issue as the other components can be accounted for by using the Rietveld method that provides the ability to separate all contributions to peak intensities [7,8]. Finally, orientation effects, which are observed in reflection geometry, can be overcome through rocking of the entire cell back and forth through a large angular range in transmission geometry [9,10].

Due to the greater need for low absorption of X-rays in a transmission *in-situ* cell, compared to in reflection mode, their use was only made possible through the use of a thin lithium metal anode and polymer electrolytes, which act to minimise X-ray absorption [11]. Transmission experiments became significantly easier upon the development of the Bellcore plastic lithium ion cell [12]. A cell in the original PLIon™ design consists of five layers: a copper grid current collector, a carbon based negative electrode laminate, a thin polymer separator which can swell to accommodate the electrolyte, a positive electrode laminate and an aluminium grid current collector. The whole assembly can be thermally fused together in air to form a single unit. The plasticiser in the laminate is then removed at a later stage by using ether. This creates pores into which the electrolyte can be injected while under an inert atmosphere. The entire cell can then be thermally sealed inside a metal–plastic laminate bag (typically aluminium coated and only around 25 μm thick). The overall thickness of the whole cell is around 300 μm, making it well suited to transmission type experiments. This particular design has been used frequently with researchers adapting the cell to suit their needs [9,13–15]. All of the cell designs mentioned so far were used in conjunction with conventional X-ray diffractometers. Due to the fixed wavelengths of conventional diffractometers and the long collection times required to obtain sufficient counting statistics the types of experiments performed and available cell designs are somewhat limited. This is why the true potential of transmission *in-situ* cells was only realised through their combination with synchrotron X-ray radiation.

The ability to select the specific X-ray energy and beam size is made possible with synchrotron sources which opened up a great deal of flexibility in cell design. If required a high energy (short wavelength) beam can be used so that attenuation is not as significant as it is with conventional X-ray powder diffractometers. In addition, the amount of time required per pattern is substantially reduced. When combined with either an area or a curved position sensitive detector rapid collection of whole diffraction patterns (over a large 2θ range) in minutes becomes possible, allowing continuous data collections, and time-resolved *in-situ* investigations [13,16–18]. One example making particularly good use of the highly collimated, small beam size available at a synchrotron X-ray source was the work performed by Morcrette et al. on $LiCoO_2$ [10]. In this study a confined (0.2×0.2 mm) beam was used in conjunction with an image plate detector. A standard Bellcore-type plastic cell was used with a small hole in the copper grid to allow the diffracted X-rays out of cell. The micro X-ray beam was then aligned so as to pass through the smaller holes in the aluminium grid. In order to reduce preferred orientation effects diffraction images were taken with the cell in six positions. This procedure effectively removes all contributions from the metal current collectors which would ordinarily dominate the resulting diffraction patterns.

There are several cell designs which have been modified to suit both reflection and transmission geometries, or were originally designed for reflection geometry and have since been modified for use in transmission mode. One such design, which is still in wide use today due to the extremely simple handling and ease of cleaning, are Swagelok™-type cells. In a typical Swagelok™ cell the body is screwed into a stainless steel block which can act to hold a beryllium window in place. The body is in contact with the positive electrode while the negative electrode is supported by a spring on a plunger which is electrically isolated from the inner wall of the body [19]. The Swagelok™ type cell has been widely adapted to fit in reflection [5] and, more recently, transmission modes [20,21].

However, Swagelok™ cells need to be custom made to fit the intended instrument, and/or a specialised holder made.

Finally, there are a larger variety of cells which do not necessarily fit into the above cell-type categories but have similarities with most of the above designs. These have been custom made to suit the particular needs of an experiment and so are not widely used. However, there is much that can be learnt and considered from their design. Recently the use of Kapton tape as an X-ray transparent window has become common. While it does not provide a perfectly air-tight seal it does keep out moisture for a few days making it more suited to the rapid collection times achievable at synchrotron X-ray sources. It is also much cheaper and safer to handle than including a beryllium window in the cell design. A common example is taking a standard coin cell and drilling a hole in either the positive electrode side (for reflection) [22,23] or through both sides (transmission) [24] and sealing the holes with Kapton tape. One example is a coin cell made by Rhodes et al. [22] which places the Kapton tape on the inside of the punched can and is then sputtered with aluminium to act as a current collector. Sputtering with aluminium also prevents the transfer of moisture through the Kapton tape. In addition, the sputtering technique produces an ultra thin layer (300 nm) significantly minimising the potential beam attenuation due to Al.

1.2. Rationale and specific considerations

Despite the large number of groups performing *in-situ* experiments over the last three decades, *in-situ* cells have not converged to a single ideal design. This is largely due to the fact that each cell needs to be carefully designed to meet its intended purpose and to fit the experimental set-up available on a particular X-ray instrument. Thus, especially for researchers hoping to utilise *in-situ* methods to study the formation of new meta-stable phases expressly for the purpose of fundamental structural investigations, designing an *in-situ* cell is not at all trivial. As mentioned above, many *in-situ* cells can be of a complex design, aiming to maximise both electrochemical properties whilst still obtaining a high quality diffraction pattern. Fortunately, for structural studies it is likely that only a single charge/discharge is needed to produce the desired phase, which reduces the need for complex cell sealing. Further, the cell does not necessarily need to be electrochemically optimised, so long as the conversion of the structure is homogeneous in the region that the X-ray beam probes. However, care must be taken to ensure that the resulting diffraction pattern can be used for high quality structural analysis and that every phase observed can be identified. Finally, the benefits of performing *in-situ* experiments at a synchrotron source far outweigh the main disadvantage, which is availability. Given that many powder diffraction beamlines have been optimised to allow for complex *in-situ* experiments (not just limited to lithium ion battery research) it is significantly advantageous to carefully design an *in-situ* cell for a synchrotron source. With this in mind and by considering the most ideal features of previous *in-situ* cells, the details of an *in-situ* cell designed for use on the powder diffraction beamline at the Australian Synchrotron are presented. The lithium insertion material which forms the basis of this study is the defect perovskite $Li_{0.18}Sr_{0.66}Ti_{0.5}Nb_{0.5}O_3$ [25]. $Li_{0.18}Sr_{0.66}Ti_{0.5}Nb_{0.5}O_3$ exhibits favourable lithium insertion characteristics as well as the ability to reversibly insert more than one lithium ion per vacant *A*-site in the structure, making it an interesting example to investigate *in-situ*.

2. Experimental

Polycrystalline samples of $Li_{0.18}Sr_{0.66}Ti_{0.5}Nb_{0.5}O_3$ were prepared by heating stoichiometric amounts of Li_2CO_3 (Merck, 99%), $SrCO_3$ (Aldrich, 99.9+ %), TiO_2 (Aithaca, 99.995%) and Nb_2O_5 (Aithaca, 99.998%) to 950 °C for 15 h. Pressed pellets were then heated at 1190 °C for 48 h and quenched in air. The resulting active material was then mixed with carbon black and Teflon™ in a 75:15:10 weight ratio in *N*-methylpyrrolidone (NMP) (Sigma Aldrich, 99.5%) to form a slurry which was spread onto a 18 μm thick copper sheet using a 400 μm notch bar, creating a wet cathode film of ~380 μm thickness. The NMP was then evaporated by heating to 70 °C overnight in a vacuum oven. The prepared cathode was transferred into an argon filled glove box and cut into 1 × 1 cm squares, with an electrode loading of ~6.0(1) mg cm^{-2} for use in the *in-situ* cell.

All cell components were machined in-house using readily available materials. The *in-situ* cell was designed to be used in transmission mode and so comprised of two aluminium plates, one with a small recess (1.2 × 1.2 × 0.2 cm) and the other with a raised section with slightly smaller dimensions. On one side a small 0.2 × 0.4 cm rectangular entry hole was cut and on the other side a larger 0.4 cm diameter hole was drilled. Each half of the cell casing was electrically insulated from the other using Kapton tape, which also acted to seal the windows in the casing. The cell was assembled using a lithium foil anode (200 μm), poly(vinylidene fluoride) (PVDF) separator, the active material deposited on copper and 1–2 drops of 1 M $LiPF_6$ in 1:1 (v/v) ethylenecarbonate:dimethylcarbonate electrolyte. The whole cell was assembled as shown in Fig. 1 with the beam direction specified. Each electrode was placed so as to be in indirect electrical contact with its half of the casing so that the case itself acted as the current collector. That is, to avoid Li–Al alloying the lithium metal anode was only in contact with a thin copper foil which in turn was in direct contact with the aluminium. The plates were held together using insulating screws and the edges sealed with wax.

Cycling of the cell was performed using a Solartron SB1210 galvanostat/potentiostat. Cells were cycled under a constant current regime with a rate of 1.7(1) mA g^{-1}. High resolution synchrotron X-ray powder diffraction (XRD) patterns were collected *in-situ* on the powder diffraction beamline, 10-BM-1, at the Australian Synchrotron using the MYTHEN microstrip detector [26] and a Si(111) monochromator. Using LaB_6 (NIST standard 660a) the wavelength was accurately determined to be 0.82605(1) Å. LaB_6 deposited on copper was then used to define the zero position enabling copper to be used as an internal standard for the cell. The

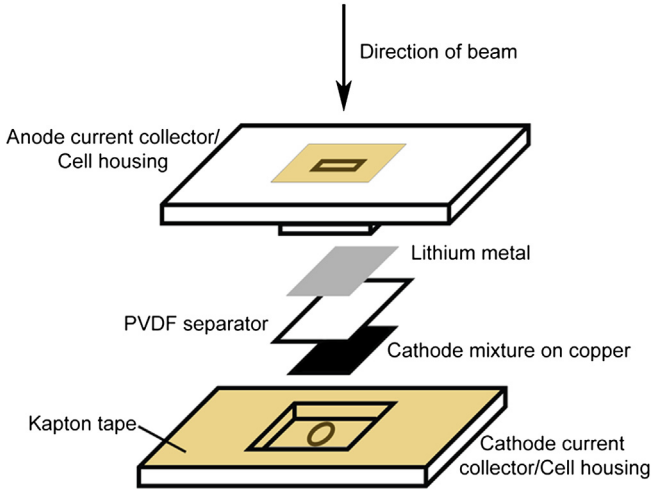

Fig. 1. Exploded view of the electrochemical cell used in the diffraction experiments. The two halves are held together using insulated screws (not shown). The aluminium casing serves as the current collector and so electrical contacts can be placed on either side of the cell to attach to a galvanostat.

cell was mounted on a simple holder which was mounted onto an XYZ stage and oriented such that the beam entered through the smaller window (Fig. 2). Data were collected in two 80° frames (*i.e.* detector position 1 and position 2) across the 2θ range 2–82.5°, with the frames shifted by 0.5° in order to cover the 0.2° gaps between the modular detectors approximately every 5°. Each detector position was collected for 3 min and the time between frames was 18 s. The sample stage was rocked over a 12° angular range during data collection to reduce preferred orientation effects. Prior to analysis, the data obtained from the two detector positions were spliced. That is, data from each position were normalised against a common reflection then the gaps from position 1 were filled with data from position 2 resulting in a dataset over the 2θ range 2–82.5° (note that for scattering angles higher than $2\theta = 50°$ the edge of the window on the cell attenuated the X-ray beam). Sequential Le Bail fitting was performed using the General Structure Analysis System (GSAS) in combination with EXPGUI [8,27].

3. Results and discussion

In-situ cells containing $Li_{0.18}Sr_{0.66}Ti_{0.5}Nb_{0.5}O_3$ prior to discharge had an open circuit voltage of 2.57 V. A comparison of the initial diffraction pattern prior to discharge and the active material collected prior to inclusion in the cell is provided in Fig. 3. The major additional reflections appearing in the *in-situ* diffraction pattern that are not in the pristine material's pattern are due to copper from the current collector, marked with asterisks, and a single peak from the aluminium housing. Due to the high resolution

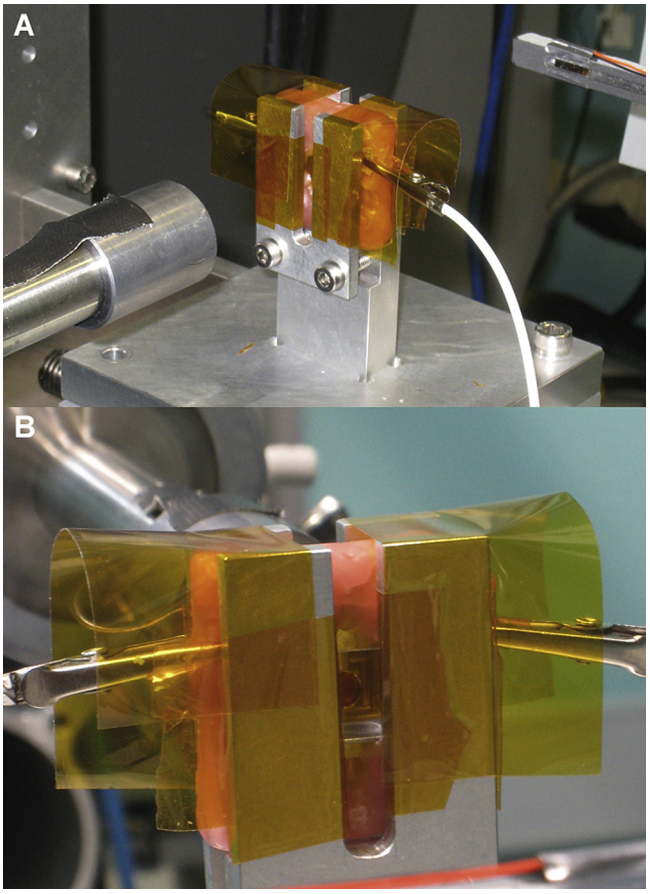

Fig. 2. A: *In-situ* cell mounted on a specially designed cell holder on an XYZ stage. The beam enters from the front face shown and exits from the other side. B: View of the cell from the back, showing the X-ray transparent window.

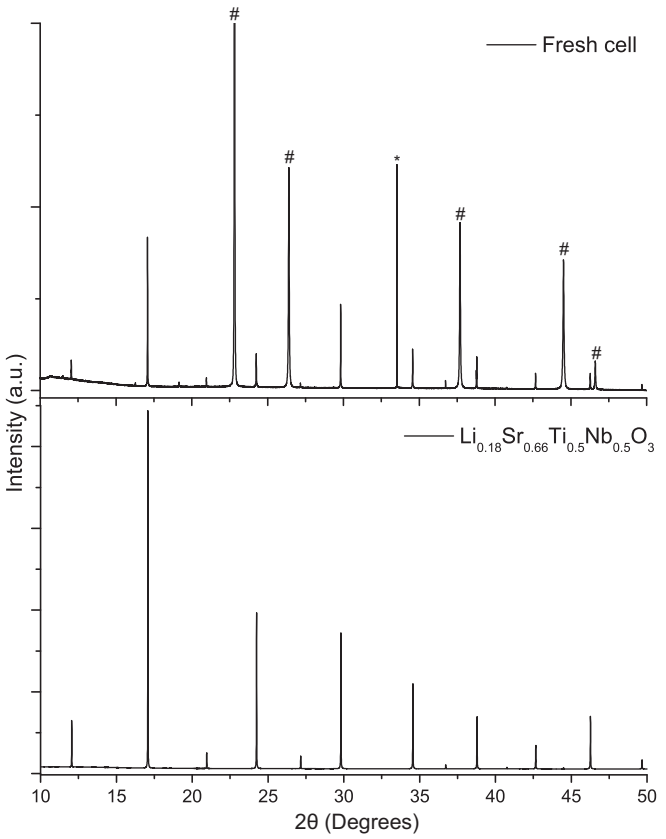

Fig. 3. Synchrotron XRD patterns of the fresh cell compared against pure $Li_{0.18}Sr_{0.66}Ti_{0.5}Nb_{0.5}O_3$. Peaks arising from the copper current collector are marked with a hash and the one from the aluminium casing with a star. Due to the significantly higher intensity of the copper reflections, the top pattern has been cropped at the top for clarity reasons.

afforded by the MYTHEN detector, all phases are clearly resolved with no overlapping peaks present, allowing accurate phase identification. Further, the active material diffracts with an excellent signal-to-noise ratio enabling accurate determination of unit cell information, although the current collector diffracts more strongly.

The changes which occurred during cycling were then investigated by performing sequential Le Bail fits for the 346 spliced diffraction patterns, which spanned one entire discharge/charge cycle. A plot comparing the refined cell parameters and the electrochemical profile as a function of lithium content is provided in Fig. 4. In agreement with a sloping discharge profile, $Li_{0.18}Sr_{0.66}Ti_{0.5}Nb_{0.5}O_3$ remains as a single phase cubic perovskite across the entire discharge/charge range with a total unit cell volume expansion of 1.819(2)%. The change in structure is completely reversible with the crystal lattice returning to its original dimensions on charging. In addition, the peaks remain very sharp after the full first cycle (FWHM changes from 0.0186(8)° to 0.0262(5)° for the (310) reflection). The gradual evolution of the lattice parameters during the complete cycle can be correlated with the gradual peak shifts, shown in Fig. 5 for the (321) reflection of the perovskite material relative to the copper (222) reflection.

There is excellent agreement between the variations in cell parameters and the electrochemical profile with correlated features, as indicated in Fig. 4. Given the close correlation of electrochemical profile and refinement parameters in regards to time it becomes possible to extract time resolved information for the structure as a function of voltage output. A linear fit to cell parameters over the entire discharge process results in a rate of change of cell parameters of $1.840(9) \times 10^{-5}$ Å min^{-1} with an *R*-squared value of 0.9956.

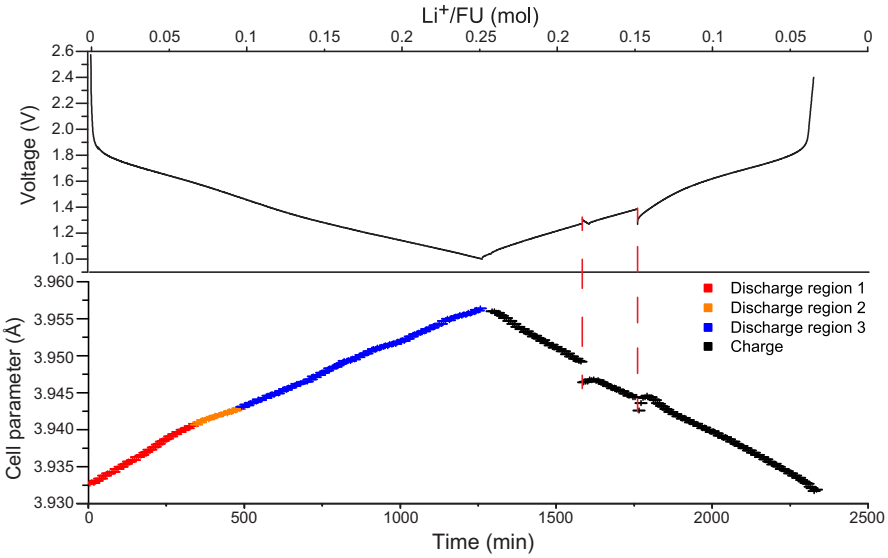

Fig. 4. Top: discharge and charge cycle for the *in-situ* cell. Bottom: the change in cell parameters as a function of discharge. The three regions corresponding to three different rates of cell parameter change are indicated by the red, orange and blue data points. The red dotted lines confirm that disruptions to the electrochemistry correlate with changes to the cell parameter induced through relaxation effects. (For interpretation of the references to colour in this figure legend, the reader is referred to the web version of the article.)

However, the fit of this line to the cell parameters at the start of discharge is quite poor. In this region, a change in the slope after 350 min (1.58 V) and then again after 480 min (1.47 V) is observed. Thus, three separate linear fits are used, the regions for which were selected based on the quality of each linear fit. These three regions had rates of change of $2.47(1) \times 10^{-5}$ Å min^{-1} (region 1), $1.44(5) \times 10^{-5}$ Å min^{-1} (region 2) and $1.765(6) \times 10^{-5}$ Å min^{-1} (region 3) with *R*-squared values of 0.998, 0.977 and 0.998 respectively. Thus, the rate of unit cell expansion reduced by 42(5)% between the first and second region, before increasing in the third region to a rate of expansion that was 28(5)% lower than the rate of expansion in the first region. More notably, these three regions identified in the time-evolution of the cell parameters correlate with a change in the slope of the electrochemical profile occurring at 1.55 V and 1.36 V (determined from linear fits), suggesting that the response of the structure to lithium insertion is having a direct impact on the shape of the electrochemical profile. Previous work we have performed on related defect perovskites had shown, through a combination of variable temperature synchrotron X-ray diffraction and electron diffraction techniques, that the rate of cell expansion can be directly influenced by the magnitude of dynamic Ti/NbO_6 octahedral rotations [28]. It is possible that a similar phenomenon is occurring in $Li_{0.18}Sr_{0.66}Ti_{0.5}Nb_{0.5}O_3$, albeit in response to lithium insertion rather than temperature. Further work will need to be performed in order to confirm the structural changes occurring in these three regions.

Unlike a laboratory-based XRD experiment, a synchrotron XRD experiment occasionally experiences loss of the X-ray beam. This

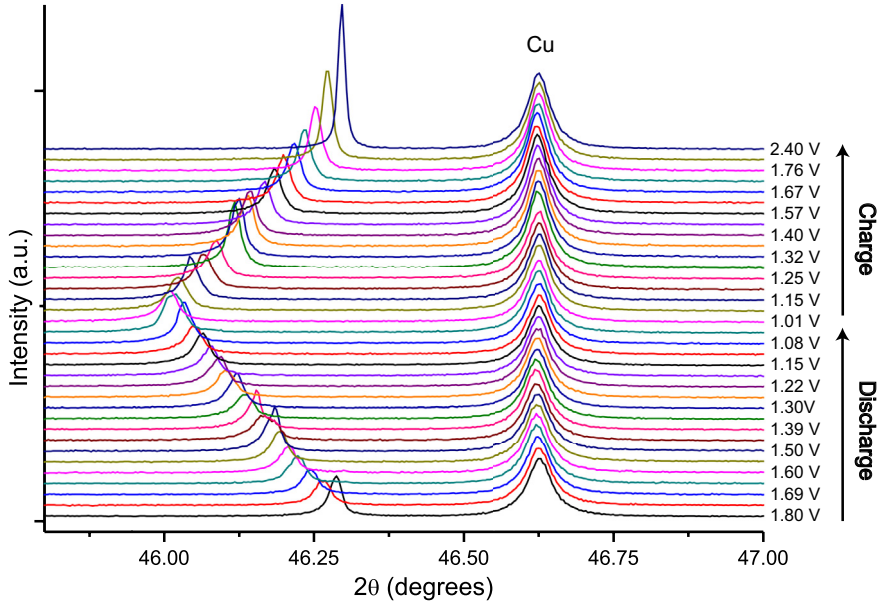

Fig. 5. Continuous evolution of the $Li_{0.18}Sr_{0.66}Ti_{0.5}Nb_{0.5}O_3$ perovskite (321) reflection relative to the copper (222) reflection. For reasons of clarity, only every 10th diffraction pattern is shown. The discharge cycle begins at the base of the plot and continues until the voltage reaches 1 V at which point the charge cycle begins. The sudden changes in intensity are due to particle averaging effects, resulting from a small beam size and particles re-orienting during cycling.

occurred twice during the almost 40 h of the *in-situ* data collection (see Fig. 4). During this time the charging process was paused, as it was not known how long the beam would be unavailable. As a result the material began to relax and the potential drifted slightly, confirming that the cell was not under equilibrium conditions during this process. The unit cell dimension reduced by 0.071(1)% for the first break (124 min) and then 0.0456(7)% for the second break (160 min). Once the X-rays were recovered the cell functioned normally and the structural parameters could be determined. Ultimately, this loss did not change the major features reported as the slope of the change in cell parameters before and after the beam losses were very similar ($2.41(2) \times 10^{-5}$ from 1 to 1.27 V and $2.22(2) \times 10^{-5}$ from 1.47 to 2.4 V, both with an R^2 of 0.996). In addition, the electrochemical profile overall is consistent with one that was previously recorded [25].

Thus, by using the *in-situ* cell we were successful in elucidating accurate information on rate characteristics within the first electrochemical cycle. In order to better understand what causes the changes in the rates of unit cell expansion, full Rietveld analysis will need to be performed. However, in the present case there were difficulties encountered with particle averaging effects due to the small size of the beam (1×3 mm). This can be seen by comparing the two reflections at $2\theta = 24.3^\circ$ and 29.8° in Fig. 3. In the pristine $Li_{0.18}Sr_{0.66}Ti_{0.5}Nb_{0.5}O_3$ sample, the reflection at $2\theta = 29.8^\circ$ is slightly lower in intensity compared to the one at $2\theta = 24.3^\circ$, whereas in the diffraction pattern from the cell it is much more intense. As the sample is a cubic perovskite, preferred orientation effects are ruled out. Thus, in future iterations of the cell a larger window in combination with a larger beam size will be used. This has the added benefit of allowing for a larger 2θ range to be accessed. That is, despite the MYTHEN detector allowing for data to be collected over an 80° 2θ range, data was only collected over 50°. This was because at scattering angles higher than $2\theta = 50^\circ$ the edge of the window on the cell attenuated the X-ray beam.

One final consideration is the effect of splicing the data from the two detector positions, as was performed for the sequential analysis. As the structure is continuously changing there is the possibility of a mismatch in peak positions between the two detector positions. In the current study this shift was determined to be small enough to ignore (*e.g.*, a shift of 0.0001 Å for the (211) reflection) because of the slow current rate used ($1.7(1)$ mA g^{-1}). However, if a faster discharge rate is utilised, then this effect could become significant enough to cause problems in the analysis. A possible solution would be to position the detector such that no important reflections fell within one of the 0.2° gaps. Although this issue could be avoided by using an image plate detector, the MYTHEN detector provides high resolution and a large angular range, allowing for the detection of subtle changes in the rate of crystal lattice expansion demonstrated above.

4. Conclusions

A simple *in-situ* cell for fundamental structural investigations using synchrotron X-ray powder diffraction has been designed. The cell consists of few parts and does not need any specialised equipment for construction, making the design accessible to researchers who do not necessarily have a background in electrochemistry and therefore do not have standard equipment (*e.g.*, a coin cell press). The cell was highly successful for the first full electrochemical cycle, enabling continuous collection of diffraction patterns across the whole discharge–charge range for $Li_{0.18}Sr_{0.66}Ti_{0.5}Nb_{0.5}O_3$. The rapid collection times combined with the high resolution available from a synchrotron X-ray diffraction experiment enabled three separate regions in the time-evolution of the cell parameter during discharge to be identified. These three regions are only subtly differentiated from another by a change in the rate of crystal lattice expansion. This result exemplifies the benefit of using rapid, high resolution, continuous collection at a synchrotron X-ray source. Further, the change in unit cell expansion corresponds to inflections in the voltage profile, suggesting that the structural feature which is inducing the change in the unit cell expansion is also influencing the voltage output. In order to investigate this further the cell will need to be modified in order to reduce the particle averaging effects by, *e.g.*, making the window larger and using a larger beam size as well as rocking the sample over a wider angle. Doing so will enable a full sequential Rietveld refinement to be performed.

Acknowledgements

A part of this work was carried out on the powder diffraction beamline at the Australian Synchrotron, Victoria, Australia. The authors would like to thank AINSE Ltd for providing financial assistance through the postgraduate award and research fellowship schemes. The authors would also like to acknowledge the technical support from the Bragg Institute, Australian Nuclear Science and Technology Organisation and the School of Chemistry, University of Sydney.

References

[1] G.G. Amatucci, J.M. Tarascon, L.C. Klein, J. Electrochem. Soc. 143 (1996) 1114–1123.
[2] X.Q. Yang, X. Sun, S.J. Lee, J. McBreen, S. Mukerjee, M.L. Daroux, X.K. Xing, Electrochem. Solid State Lett. 2 (1999) 157–160.
[3] R.R. Chianelli, J.C. Scanlon, B.M.L. Rao, J. Electrochem. Soc. 125 (1978) 1563–1566.
[4] J.R. Dahn, R.R. Haering, Solid State Commun. 40 (1981) 245–248.
[5] S. Boyanov, D. Zitoun, M. Ménétrier, J.C. Jumas, M. Womes, L. Monconduit, J. Phys. Chem. C 113 (2009) 21441–21452.
[6] M.N. Richard, I. Koetschau, J.R. Dahn, J. Electrochem. Soc. 144 (1997) 554–557.
[7] V. Petříček, M. Dušek, L. Palatinus, Jana2006, The Crystallographic Computing System, Institute of Physics, Praha, Czech Republic, 2006.
[8] A.C. Larson, R.B. Von Dreele, Los Alamos National Laboratory Report, 2000, pp. 86–748.
[9] O. Bergstrom, T. Gustafsson, J.O. Thomas, J. Appl. Crystallogr. 31 (1998) 103–105.
[10] M. Morcrette, Y. Chabre, G. Vaughan, G. Amatucci, J.B. Leriche, S. Patoux, C. Masquelier, J.M. Tarascon, Electrochim. Acta 47 (2002) 3137–3149.
[11] T. Gustafsson, J.O. Thomas, R. Koksbang, G.C. Farrington, Electrochim. Acta 37 (1992) 1639–1643.
[12] J.M. Tarascon, A.S. Gozdz, C. Schmutz, F. Shokoohi, P.C. Warren, Solid State Ionics 86–88 (Part 1) (1996) 49–54.
[13] R.-Z. Yin, Y.-S. Kim, S.-J. Shin, I. Jung, J.-S. Kim, S.-K. Jeong, J. Electrochem. Soc. 159 (2012) A253–A258.
[14] C. Lampe-Oennerud, J.O. Thomas, M. Hardgrave, S. Yde-Andersen, J. Electrochem. Soc. 142 (1995) 3648–3651.
[15] B. Gérand, A. Blyr, A. Du Pasquier, J.B. Leriche, L. Seguin, J. Power Sources 81–82 (1999) 922–924.
[16] M.R. Palacín, F. Le Cras, L. Seguin, M. Anne, Y. Chabre, J.M. Tarascon, G. Amatucci, G. Vaughan, P. Strobel, J. Solid State Chem. 144 (1999) 361–371.
[17] M.R. Palacín, G.G. Amatucci, M. Anne, Y. Chabre, L. Seguin, P. Strobel, J.M. Tarascon, G. Vaughan, J. Power Sources 81–82 (1999) 627–631.
[18] M.R. Palacín, Y. Chabre, L. Dupont, M. Hervieu, P. Strobel, G. Rousse, C. Masquelier, M. Anne, G.G. Amatucci, J.M. Tarascon, J. Electrochem. Soc. 147 (2000) 845–853.
[19] J. Gural, J.-B. Leriche, M. Morcrette, J.-M. Tarascon, US Patent US20020192121A1 (2002).
[20] J.B. Leriche, S. Hamelet, J. Shu, M. Morcrette, C. Masquelier, G. Ouvrard, M. Zerrouki, P. Soudan, S. Belin, E. Elkaim, F. Baudelet, J. Electrochem. Soc. 157 (2010) A606–A610.
[21] T. Gross, T. Buhrmester, K.G. Bramnik, N.N. Bramnik, K. Nikolowski, C. Baehtz, H. Ehrenberg, H. Fuess, Solid State Ionics 176 (2005) 1193–1199.
[22] K. Rhodes, R. Meisner, Y.-G. Kim, N. Dudney, C. Daniel, J. Electrochem. Soc. 158 (2011) A890–A897.
[23] C.R. Fell, M. Chi, Y.S. Meng, J.L. Jones, Solid State Ionics 207 (2012) 44–49.
[24] H.C. Shin, S.B. Park, H. Jang, K.Y. Chung, W.I. Cho, C.S. Kim, B.W. Cho, Electrochim. Acta 53 (2008) 7946–7951.
[25] W.R. Brant, S. Schmid, A. Kuhn, J. Hester, M. Avdeev, M. Sale, Q. Gu, ChemPhysChem 13 (2012) 2293–2296.
[26] B. Schmitt, C. Brönnimann, E.F. Eikenberry, F. Gozzo, C. Hörmann, R. Horisberger, B. Patterson, Nucl. Instrum. Methods Phys. Res. Sect. A 501 (2003) 267–272.
[27] B.H. Toby, J. Appl. Crystallogr. 34 (2001) 210–213.
[28] W.R. Brant, S. Schmid, Q. Gu, R.L. Withers, J. Hester, M. Avdeev, J. Solid State Chem. 183 (2010) 1998–2003.